ARID ZONE JOURNAL OF ENGINEERING, TECHNOLOGY & ENVIRONMENT
AZOJETE September 2026. Vol.22(3):763-773
Published by the Faculty of Engineering, University of Maiduguri, Maiduguri, Nigeria.
Print ISSN: 1596-2490, Electronic ISSN: 2545-5818
https://doi.org/10.63958/AZOJETE/2026/22/03/017
www.azojete.com.ng

ORIGINAL RESEARCH ARTICLE

UPSCALING THE HARDNESS, CORROSION AND STRUCTURAL STABILITY OF CHLORIDE BASED INDUCED COATING VIA ECOFRIENDLY CONSTITUENTS

O.S.I. Fayomi[1,2*]

[1]Department of Mechanical Engineering, Bells University of Technology. Ota Nigeria
[2]Department of Mechanical Engineering Science, University of Johannesburg, Auckland Pack, Kingsway Campus, Johannesburg, South Africa
Corresponding author's email: ojosundayfayomi3@gmail.com

ARTICLE INFORMATION

Received: 16th June 2026
Revised: 12th August 2026
Accepted: 20th August 2026

Keywords:
Coating
Corrosion
Enhancement
Hardness
Protective

ABSTRACT

This subject of this study was the combination of zinc oxide coatings combined with unripe plantain peel particulates on mild steel. ASTM A795 mild steel was used as the subject substrate with the goal of enhancing its ability to resist corrosion. Zinc anodes as well as varying amounts of UPP particulate ranging from 0-9g/L were employed during an electrodeposition technique. A uniform voltage of 0.5 V, a temperature of 42°C, a current density of 1.5 A/cm^2 and a deposition period of 15 minutes was adopted after optimization for this work. The developed samples were characterized for hardness, microstructure and electrochemical studies. The hardness responses were evaluated using a Rockwell hardness tester in accordance with ASTM E18, while corrosion behaviour was investigated using linear sweep potentiodynamic polarization following ASTM G5. From the outcome, excellent enhancement was seen all through the coated developed alloys performance of the coated samples compared with the uncoated control sample. The microhardness rate improved from 62.5 HRB for the control sample to 66.1 HRB for the treated alloy, signifying improved mechanical and structural properties. Corrosion study exposed a decrease in corrosion rate and corrosion current density with variation in absorption of unripe plantain peel constituent. The deterioration rate occurred from 0.0403 mm/yr for the as-received sample to 0.0181 mm/yr for the developed coated sample, indicating better corrosion properties. The enhanced performance was ascribed to the establishment of a robust protective mechanical and corrosion properties of mild steel.

1.0 Introduction

Studies had shown that several coating methods had been deployed for the purpose of improving metallic structure life span (King & Jin 2026; Phogat *et al.* 2026). Electrodeposition has over time, become one the most preferred methods because it is simple to setup and has a relatively low cost of production. It also produces thin films of good quality with reproducibility (Draz *et al.* 2025). Electrodeposition had also been designated in literature as a coating technique that involved the use of a conductive substrate that was immersed in a bath containing the salt of the metal to be deposited. This results in the formation of a uniform metal coating on an electrode (Protsenko 2025; Ajayi *et al.* 2025a).

Direct current (DC) and pulse electrodeposition represent the two primary kinds of electrodeposition, that had been extensively used to produce films deposition for an array of components (Pandit *et al.* 2023). DC electrodeposition was likely to form the dendritic structure in the thin film and led to an inhomogeneous surface (Fayomi *et al.* 2025). Pulse electrodeposition can effectively address this issue. During the off (resting) period, there was sufficient time for the ions to diffuse on the electrode surface as well as for crystal formation at the alloy surface (Fayomi 2025; Akpan *et al.* 2022).

Generally, the appropriate material for coating and procedure parameters, such as coating temperature, time of deposition, material constituent concentration, optimum pH, mixing rate, average current density, and coating voltage needed to be carefully selected when preparing the coating electrolytic bath (Al-Amiery *et al.* 2023). These variables have an impact on how well coatings perform. For instance, mixing rate at a suitable temperature assisted in dissolving the different parts of the bath homogeneously. Also, an adequate stirring rate can assist overall electrophoresis, particulate mass movement toward the untreated sample, and granular disintegration (Antunes *et al.* 2014; Anwar 2021). The stirring of the bath components also prevented particle agglomeration. Similarly, coating thickness and coating time can occasionally be proportionate. Several process-related variables often influenced materials' mechanical properties, deterioration effect, crystalline behaviour, electrical, and other features (Ates 2016; Fayomi & Popoola, 2012).

The piping networks in sprinkler systems are usually made of mild steel. Mild steel was usually due to its strength advantage, accessibility, and cost friendliness (Fenker *et al.*2024; Kadhim *et al.* 2021). During use, it reacts with the atmosphere, forming stable bonds ferrous oxides and salts which in turn results in reduced integrity. It is a known fact that does not provide complete protection as it does not take attnticipated life span into consideration. The use of stainless steel was not a sustainable alternative because of cost. Corrosion can be seen as the pipe starts weakening over wide areas, causing the gradual reduction of pipe thickness (Lou *et al.* 2018; Malatji *et al.* 2017)

The primary cause of internal corrosion of sprinkler pipes is the presence of water that is always in the pipe for use and even after use, the pipe does not usually drain completely thereby causing a reaction between oxygen and zinc. Corrosion phenomenon was well documented in sprinkler pipes. The common corrosion reaction seen in sprinkler pipes was by oxidation (Sajjadnejad *et al.* 2024). Oxygen trapped inside the pipes dissolved into water and reacted with the inner surface of piping copper or black or mild steel. This reaction produces iron oxide debris that ultimately leads to major problems such as obstruction of the sprinkler pipe, sprinkler plugging, pinhole leaks, short service life, repair costs, property damage, and business disruption (Shibli *et al.* 2015).

As a fire-resistant structure, sprinkler networks are usually used in building protection. With time, mineral deposits and microbial growth within the sprinkler pipes affects their performance. This then causes reduced flow rates and can even result in system failure. For this reason, the development of surface-active coatings has been proposed as a potential solution. Therefore, this study provided a pilot assessment of a coating system developed with waste material constituent with the view of improving functionality and durability in application.

2. Materials and Method

The materials used in this study were procured from Ogun State, Nigeria and comprised ASTM A795 Grade A mild steel coupons (50 × 20 × 3 mm), zinc bars (99.9% purity, 150 × 50 × 10 mm) used as the soluble anodes, and unripe plantain peels. 2 kg of fresh unripe plantain peels were collected, washed, dried, pulverized, and processed into particulates for incorporation into the coating. The unripe plantain peel particles were incorporated as a bio-based reinforcing phase owing to their demonstrated ability to enhance the hardness, microstructural stability, and corrosion resistance of zinc-based composite coatings (Ben & Olubambi, 2024). The mild steel and Zinc anode were selected because of the applicability, low cost and inherent responses against corrosion. The steel metallic structure was 0.241% carbon and 98.514% iron, with the properties making it appropriate for advanced applications.

Zinc anodes sized of 85 × 50 × 15 mm, and cathode pieces measuring 50 × 25 × 2 mm were coupled with an electrical sectional precision machine. The steel samples were polished with emery paper to obtain smooth surfaces. They were then degreased in 0.012 M sodium carbonate solution, rinsed with distilled water, and air-dried prior to electrodeposition. The zinc anodes were similarly cleaned using the same procedure (Ajayi *et al.* 2025b).

This study employed synthesized unripe plantain peel fibers because of their inherent chemical constituent, economic and environmental viable characteristics. A Panasonic mixer (MX-GX1561 – 400 W) was utilized to blend the peels, which were subsequently then carefully rinsed, dried in sunlight for 12 hours, and filtered in order to obtain a uniform particle size. This was suitable for homogeneous dispersion within the electrolyte bath, as finer reinforcement particles had been reported to promote uniform co-deposition, improve coating compactness, and minimize particle agglomeration during electrodeposition (Qi & Kan, 2026).

Corresponding author's email address: ojosundayfayomi3@gmail.com

Five metallic samples were prepared with different bath solution using electrolytes comprising CaO, thiourea, ZnCl, ZnO, glycerin, boric acid, KCl, and NaCl were measured and dissolved in five coating baths made with distilled water (Marcolin *et al.* 2017). The selected electrodeposition parameters, including the applied voltage (0.5 V), current density (1.5 A/cm²), bath temperature (42°C), stirring speed (200 rpm), pH (4.6), and deposition time (15 min), were adopted based on previous studies that demonstrated these conditions produced uniform, adherent, and defect-free zinc-based composite coatings while minimizing hydrogen evolution and particle agglomeration (Fayomi and Popoola, 2012).

The processed mild steel cathode was positioned between the two zinc anodes in an electrolyte solution for the purpose of the conventional electrodeposition coating. The sample of steel was hooked up to the rectifying machine's negative end, and the zinc plates were attached to its positive end. These deposition conditions were selected to ensure adequate ion transport, stable nucleation and growth of the coating, and effective incorporation of the UPP reinforcement into the Zn–ZnO matrix, as recommended for zinc composite electrodeposition systems.

After the developed alloy, thickness of the coating was done using thickness gauge. The Potentiodynamic polarization approaches had been used to evaluate dissolution resistance behaviour with Stern-Geary equation engaged to calculate corrosion rate effect. In examining the crystallographic phases, X-ray diffraction (XRD) was used while Scanning Electron Microscopy/Energy Dispersive Spectrometry (SEM/EDS) was employed to assess surface structure and elemental makeup. The microhardness examination with the help of Rockwell Hardness Tester was used to measure the coated samples' hardness qualities.

3. Results and Discussion

3.1 Thickness Gain of Coated Samples

The thickness gain of the deposition (Zn-20ZnO-UPP) is shown in Tables 1. From Table 1, a relatively constant thickness of the sample before coating is observed, with a value of 4.12 mm, except for the A4 (Zn-20ZnO-9UPP) sample, which had the highest thickness value of 4.62 mm. The samples were all at an approximate thickness of 5 mm, but the sample thicknesses were reduced due to grinding, polishing, and surface preparation procedures. After coating, the sample thickness increased, with the A1 sample having a final coating value of 4.22 mm, resulting in a 0.1 mm net gain. Moving to the higher deposition content of the A2 sample, the coating thickness increased by 0.9 mm to 5.02 mm, making it the sample with the highest thickness gain among the deposition samples. The A3 and A4 samples had relatively lower thickness gains of 0.6 mm and 0.3 mm, respectively. The data indicated that the migration of ZnO ions to the steel substrate was impeded by nano UPP particles. The process parameters could potentially influence the thickness of the deposition coatings, like in similar findings reported by (Akpan *et al*. 2022).

The investigation conducted by Fayomi *et al.* 2025 supported the findings presented in Table 1, demonstrating the measurements of coating thickness carried out using a thickness meter gauge (Model 456) with an accuracy of ±1 % and the corresponding weight gain of the specimens.

Table 1: Thickness Gain (mm) of Deposition Thickness

Sample Matrix	Thickness Before Coating	Thickness After Coating	Net gain
A1	4.12	4.22	0.1
A2	4.12	5.02	0.9
A3	4.12	4.72	0.6
A4	4.62	4.92	0.3

3.2 Hardness Test Result

The measure of the indentation force on the deposition is shown in Figures 1 which shows the hardness values of the Zn-20ZnO-UPP samples. The control had the least hardness value of 62.5 HRB. With the introduction of the Zn-ZnO coating to the surface of the steel, the hardness value increased by more than 3.5 % to 64.7 HRB. The addition of 6 g of UPP to the sample surface increased the hardness further by 4.16% in comparison to the control sample and by 0.62 % in comparison to the A1 sample. The sample with 6 g of UPP had a hardness value of 65 HRB, which was 3.3 HRB more than the uncoated steel. The final sample, A4, had a hardness value of 66.1 HRB, which was the highest among the UPP-incorporated samples. The higher hardness of the coated specimens compared with the uncoated mild steel can be attributed to the formation of a dense

Corresponding author's email address: ojosundayfayomi3@gmail.com

Zn–ZnO-UPP composite coating, which promotes grain refinement and dispersion strengthening while restricting localized plastic deformation under indentation. The incorporation of the UPP reinforcing particles further enhanced coating compactness and load-bearing capacity, resulting in improved hardness, consistent with a previous study by Luo *et al.* (2018).

Though, the stability of coatings may be affected by their thickness as noted by (Thakare *et al*., 2021), the thickest coating might not always be the best coating due to the probable existence of internal defects or micro void, which might not be very noticeable (Fenker *et al*. 2014).

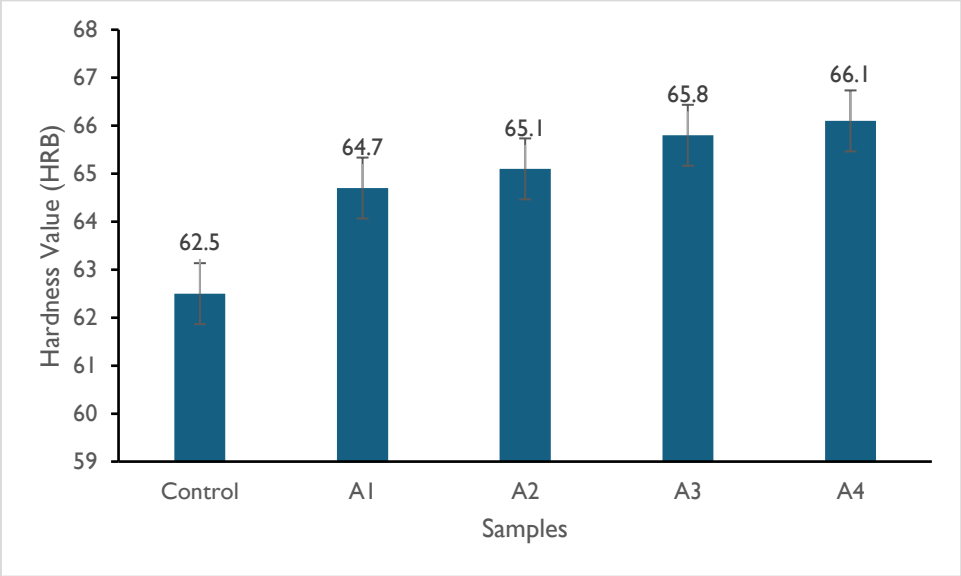

Figure 1: Hardness value for deposition

3.3 Corrosion Test Result

The electrochemical behaviour of the coated and uncoated specimens is presented in Table 2, while the corresponding open-circuit potential (OCP) and potentiodynamic polarization curves are shown in Figures 2 and 3, respectively. The uncoated specimen (Control) exhibited the highest corrosion current density (J_{corr}) of 1.95×10^{-2} A/cm² and the highest corrosion rate (0.0403 mm/yr), indicating the greatest susceptibility to corrosion. Following electrodeposition, all coated samples (A1–A4) showed lower J_{corr} and corrosion rate values than the control. The lowest corrosion rate (0.0181 mm/yr) was observed in Sample A4 (Zn–20ZnO–9UPP). This represents a 55% reduction in comparison to the uncoated specimen. This indicated that the Zn–ZnO-UPP composite coating effectively reduced the electrochemical dissolution of the steel substrate.

The OCP curves in Figure 2 showed that all coated substrates maintained stable potentials. The control specimen gradually shifted towards more negative potentials with increasing exposure time. This indicated the continued dissolution of the steel surface. On the other hand, it is observed that the coated specimens exhibited smaller potential changes, stabilizing with time. This now suggested the formation of a protective coating layer that reduced the interaction between the electrolyte and the substrate. Among the coated samples, A3 and A4 maintained the most stable potentials, indicating improved electrochemical stability.

The potentiodynamic polarization curves shown in Figure 3 further support the results in Table 2. The coated samples were observed to have lower current densities when compared with the control specimen. This confirmed a reduction in the corrosion reaction rate after the deposition of the coating. It was also noted that as the UPP content increased from sample A1 to A4, the polarization curves progressively shifted to lower current densities, demonstrating improved corrosion resistance. This behaviour suggested that the incorporation of UPP into the Zn–20ZnO matrix enhanced coating compactness and reduced the number of pathways available for the electrolyte to act on the substrate. It can then be said that the composite coating acted as an effective physical barrier, limiting charge transfer and suppressing the anodic dissolution of the steel substrate.

The combination of the effects of ZnO particles and UPP particulates is thus, the major driver of the improved corrosion performance of the Zn–20ZnO–UPP system. ZnO improved coating compactness and stability, while the UPP particles helped to fill coating defects and pores, producing a denser microstructure that limited

Corresponding author's email address: ojosundayfayomi3@gmail.com

the diffusion of aggressive ions to the steel surface. Similar improvements in corrosion resistance following the incorporation of natural particulate reinforcements into zinc-based composite coatings had been reported by Al-Amiery *et al.* (2023).

Table 2: Tafel plot of deposition

Sample	E_{corr} (V)	J_{corr} (A/Cm^2)	CR (mm/yr)	PR (Ω)
Control	-0.501	1.95E-02	0.0403	1.60E+00
A1	-0.508	1.83E-02	0.0212	1.41E+00
A2	-0.493	1.68E-02	0.0196	1.43E+00
A3	-0.487	1.51E-02	0.0184	1.41E+00
A4	-0.491	1.52E-02	0.0181	1.39E+00

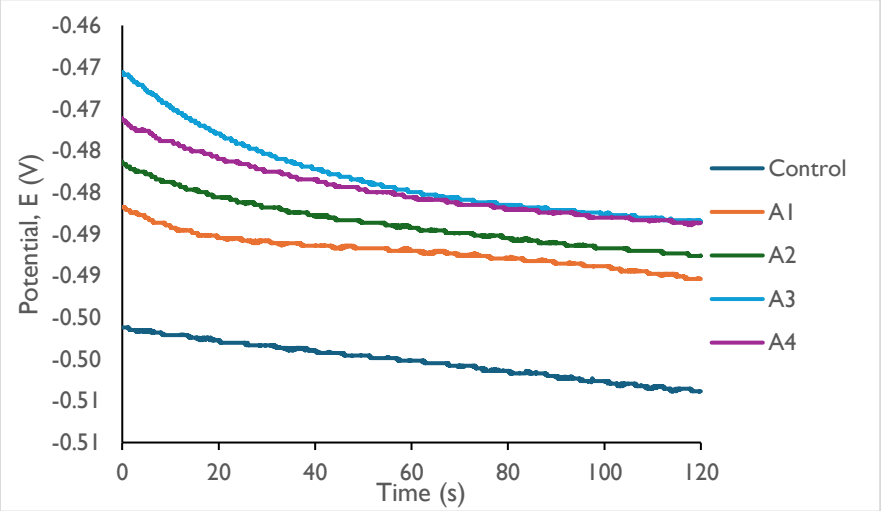

Figure 2: OCP plot of samples

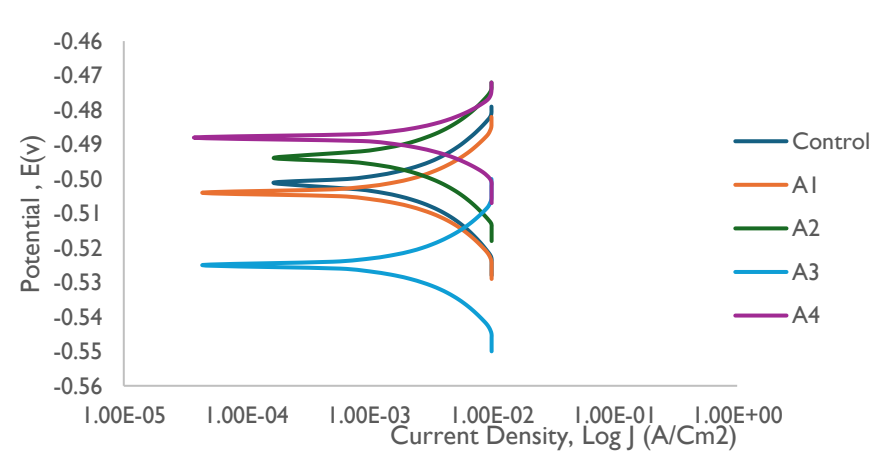

Figure 3: LSV plot of samples

3.4 Surface Micrograph

3.4.1 SEM/EDS Analysis of Coated samples

The reference steel specimen's structure was clearly homogeneous yet compacted in the SEM photograph (Figure 4). The reference sample original showed a surface's dense pattern of closely arranged fragments. Iron (Fe) and chromium (Cr) comprised the main components, based on the quantitative information on elemental composition derived from the EDS assessment of the reference sample. Fe and Cr were expressed as prominent peaks in the EDS spectra. Fe demonstrated a far higher weight percentage (75.52%) and atomic percentage (54.80%) compared to Cr (24.48% weight and 45.20% atomic).

A normal steel metal alloy, that is believed to contain considerable amounts of such metals, has this elemental makeup. The scanning electron microscope (SEM) images of the Zn-20ZnO (A1, B1) steel coating samples demonstrate notable variations in the surface structure with respect to the control sample at an average magnification of 120,000x (Figure 5). More substantial, and obvious, and more textured particulates arose as an outcome of the procedure of coating. The lesser dense and increasingly granular appearance of the surface was seen with Zn-20ZnO layer. The results of the EDS analysis of the Zn-20ZnO plated sample showed both zinc (Zn) and zinc oxide (ZnO) were deposited upon the surface of the steel. The EDS spectrum displays pronounced peaks with corresponding to zinc (Zn), oxygen (O), calcium (Ca), and carbon (C). Zn (55.45%), O (10.35%), Ca (30.00%), and C (4.20%) represent the equivalent atomic ratios for the corresponding weight percentages of Zn (50.06%), O (14.32%), Ca (30.00%), and C (5.62%). Although the existence of Zn and O reveals good ZnO formation, a significant amount of Ca reflects the inclusion of CaO within the coating operation. The natural ingredients (UPP) employed during the electrodeposition environment were probably the basis of the carbon detected (Malatji *et al.* 2017).

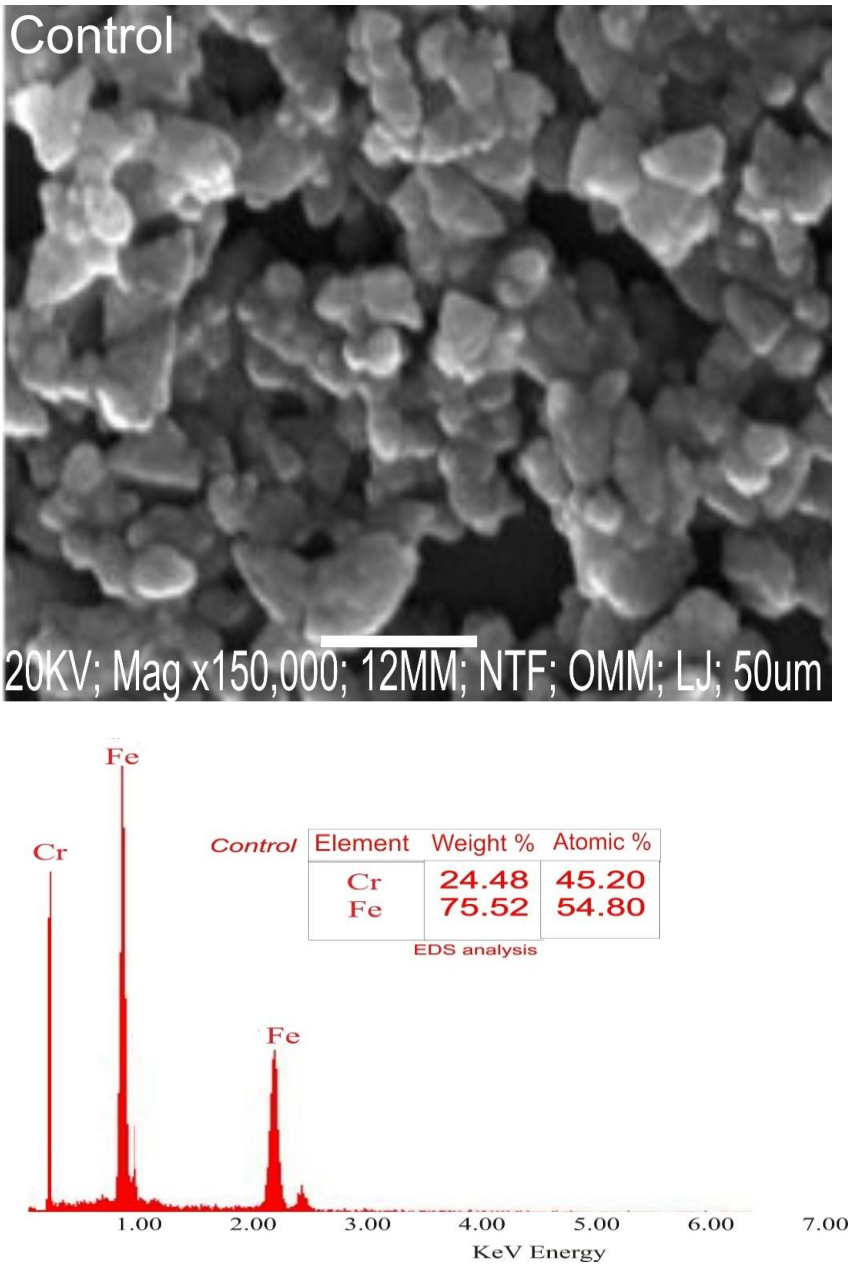

Figure 4: SEM/EDS Plot of the Control sample (As-received steel)

The steel specimen plated using (A4) Zn-20ZnO-9UPP exhibited the typical surface morphology which is notably rough and granular (Figure 6). The particulates appeared larger in size and clearer as in comparison with the reference sample, suggesting that a Zn-20ZnO-9UPP coating was effectively formed. The composition reveals an uneven surface featuring a variety of granular configurations which might result in enhanced surface features including enhanced adhesion and a typical surface area. Based on the standpoint of science, the grainy and irregular structure is triggered by the zinc ions' reaction with organic constituents of the UPP throughout

Corresponding author's email address: ojosundayfayomi3@gmail.com

the electroplating process. The emergence of Zn and ZnO crystalline by the intrinsic fibers in UPP could be accountable for the visible granular morphology.

This enhanced roughness of the surface could boost the coating's mechanical interaction and bonding ability in environments requiring strong surface characteristics. The composition of the Zn-20ZnO-9UPP specimen, as identified through EDS examination, comprises zinc (Zn), carbon (C), and oxygen (O). The weight percentages are 80.40 % for Zn, 9.25 % for C, and 20.35 % for O, while the atomic percentages are 70.30 % for Zn, 7.60 % for C, and 20.10 % for O. The significant presence of Zn in the sample confirmed the successful incorporation of zinc and zinc oxide (ZnO) onto the steel surface. The detection of C indicated the introduction of organic substances from the UPP, potentially enhancing the mechanical robustness and corrosion resistance of the coating, among other attributes. Carbon (C), Zinc (Zn), and oxygen (O) comprise the Zn-20ZnO-9UPP sample's structure, as identified by EDS examination. Atomic proportions are 7.60% for C, 70.30% for Zn, and 20.10% for O; weight percentages are 80.40% for Zn, 9.25% for C, and 20.35% for O. The sample's notable zinc content corresponds to the efficient incorporation of zinc and zinc oxide (ZnO) through the steel surface. The inclusion of C indicated an incorporation of organic components derived from UPP, that could enhance the coating's physical strength as well as resistance to oxidation, amongst other characteristics.

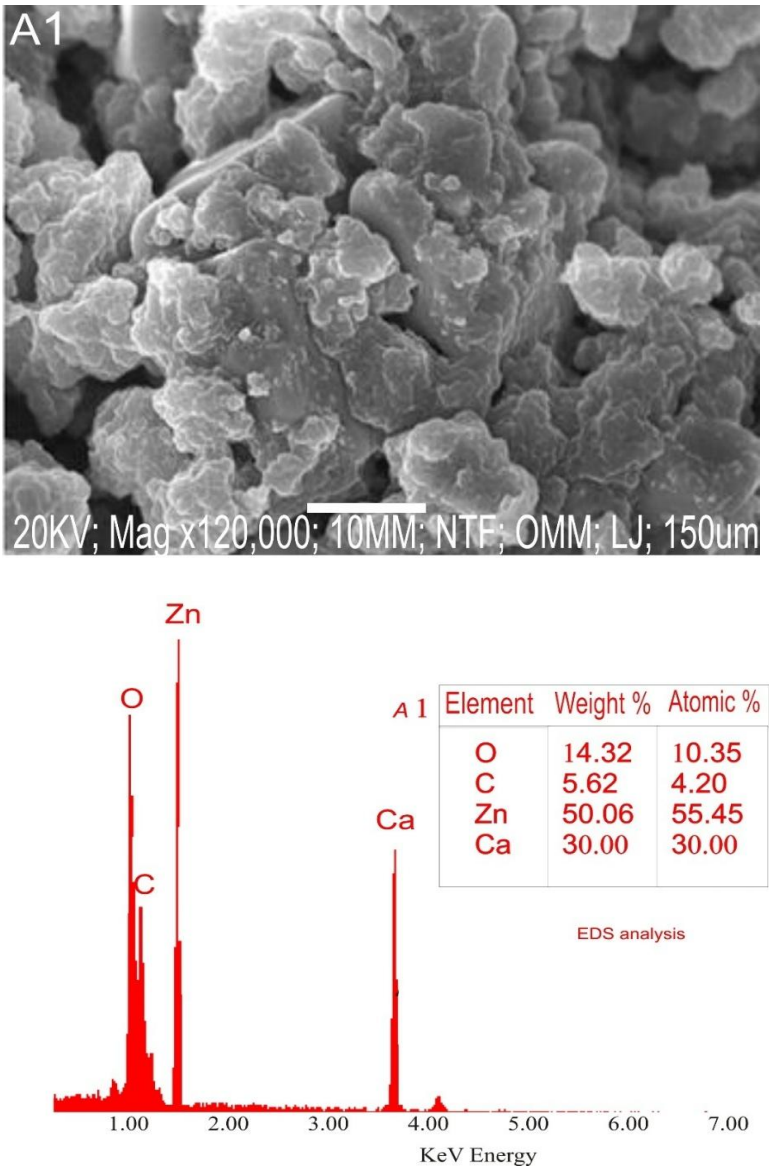

Figure 5: SEM/EDS Plot of A1 sample (Zn-20ZnO)

3.4.2 XRD Analysis of Coated Samples

Zinc (Zn) as well as zinc oxide (ZnO), aluminum oxide (Al2O3), calcium carbonate (CaCO3) and silicon dioxide (SiO2), are all shown as distinct peaks in the XRD analysis of the A1 sample (Zn-20ZnO) (Figure 7). It is important to note that this successful deposition of zinc and zinc oxide onto the steel substrate was

confirmed by the existence of Zn and ZnO peaks. ZnO's unique peak patterns at 2θ levels at 36°, 38°, and 65° showed its crystalline composition. Importantly, the peak at 44° suggested the possible formation of metallic Zn in its pure form. SiO_2 and Al_2O_3 phases analysis showed potential interactions with the steel substrate throughout the coating operation, suggesting a likelihood of contaminant or subsequent phase constituent. With respect with to the A1 sample, peaks comparable to those seen in the XRD structure of the A4 sample (Zn-20ZnO-9UPP) also became visible, displaying more distinctive characteristics (Figure 8). The continuing noticeable peaks linked to Zinc and Zinc oxide implied the presence of the primary coating constituent (Fayomi & Popoola, 2012). Nevertheless, the phenomenon showed peaks that represented secondary peaks involving calcium magnesium sulfate ($CaMg_2(SO_4)_4$) and silicon disulfide (Si_2S_2) and the interface.

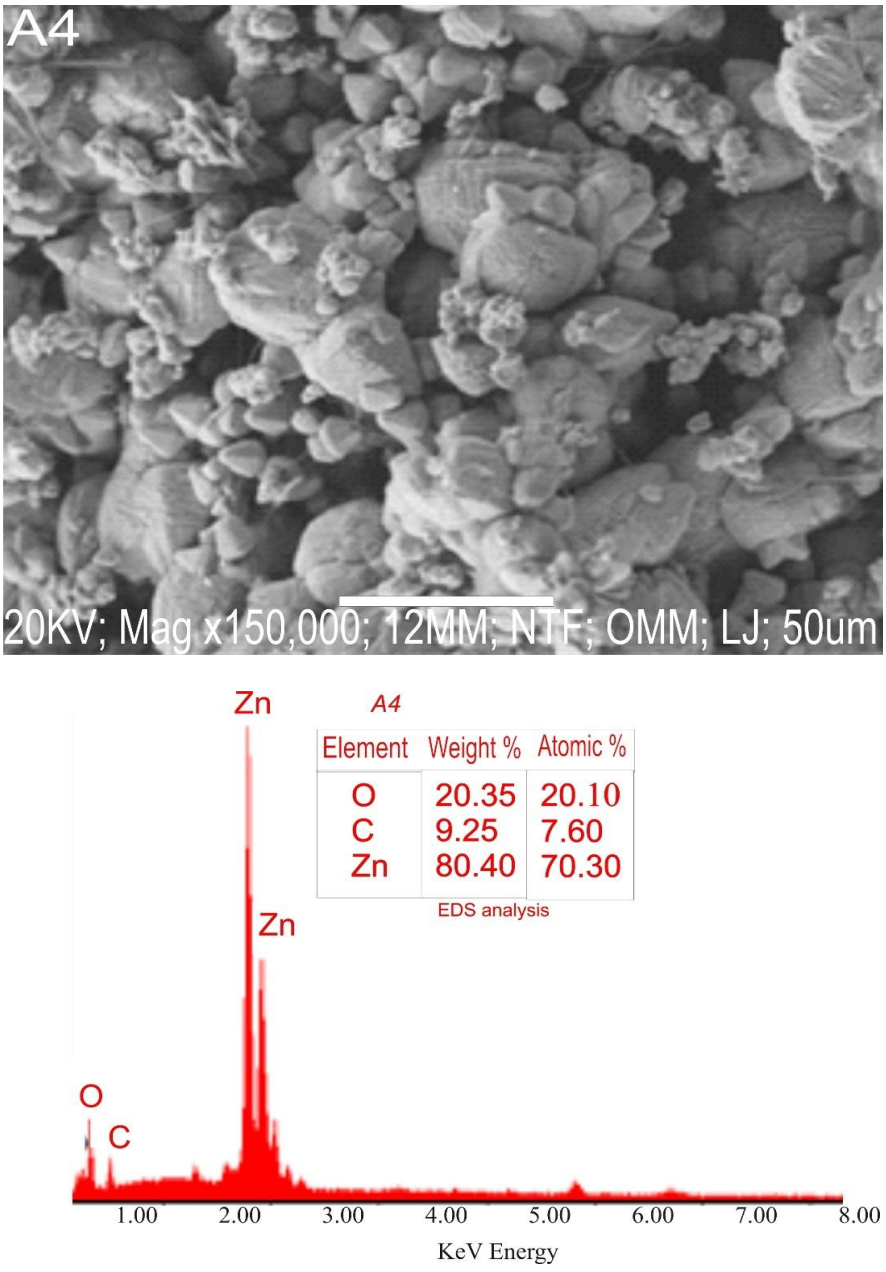

Figure 6: SEM/EDS Plot of A4 sample (Zn-20ZnO-9UPP)

Since the film incorporated unripe plantain peel particulates (UPP), the identification of the corresponding additional phases suggested the existence of new compounds and components of inhibit tendency. The inclusion of UPP might make it more convenient to implement complex sulphates and oxides, that could boost the aforementioned coating's entire chemical degree of complexity (Kadhim *et al.* 2021). The intermetallic with the help of XRD revealed complex relationships among the coatings' metallic, oxide, and organic material constituents. Each sample can be seen to exhibit the presence of Zn and ZnO peak values, that are essential for providing a fundamental barrier towards corrosion mitigation. By introducing CaO and UPP, intermetallic phases such as $CaZnO_3$, $CaMg_2(SO_4)_4$, and Si_2S_2 were seen, displaying chemical reactions which could enhance coatings' structural, mechanical and chemical resilience. The multifaceted complexes created

as results of the organic particles (UPP) supported the coatings' overall efficacy by functioning as environmentally friendly inhibitors. These findings emphasized the likelihood of utilizing natural reprocessed biowaste products to develop advanced, adaptive coatings of protection for steel, by boosting both durability and resistance against ecological corrosion effect.

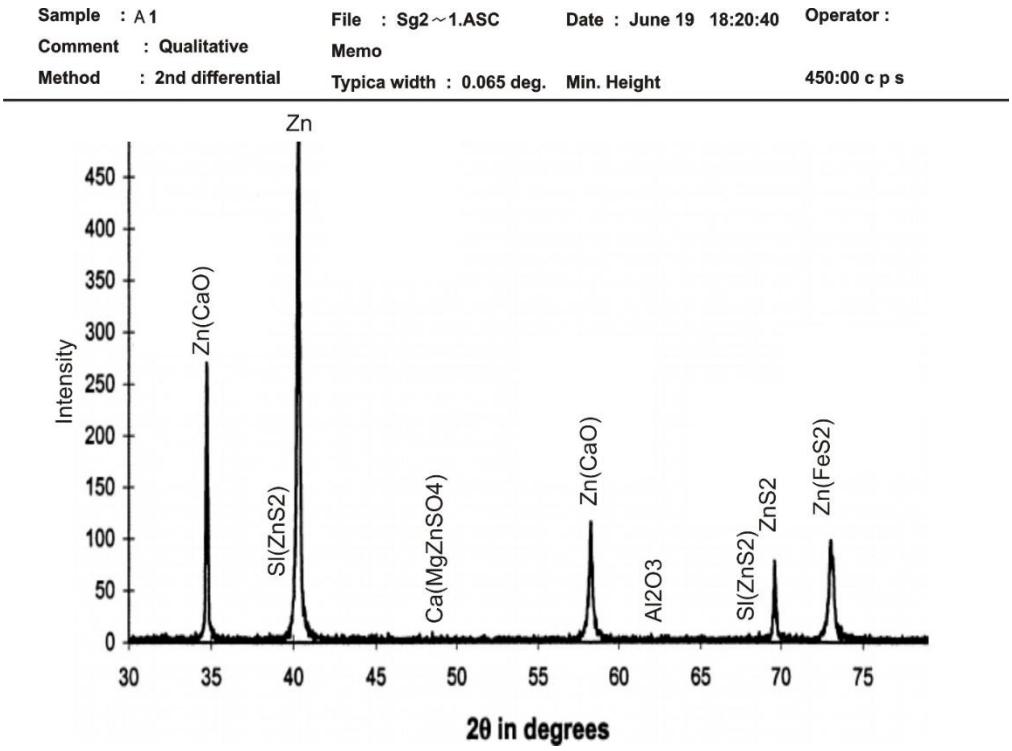

Figure 7: XRD Plot of A1 sample (Zn-20ZnO)

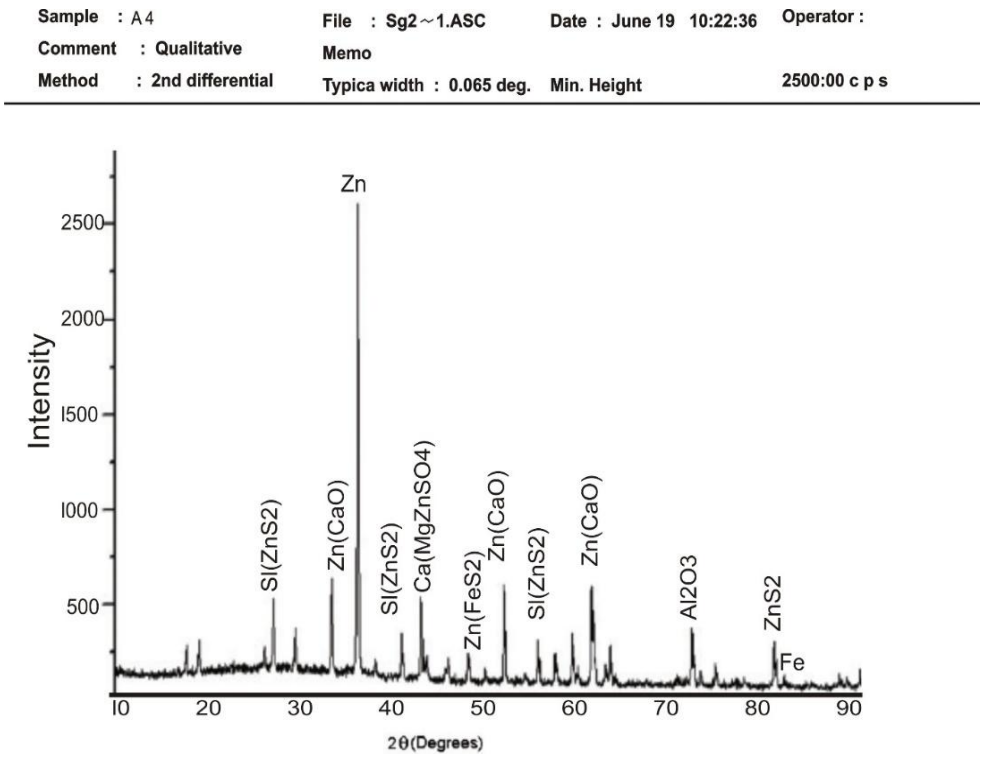

Figure 8: XRD Plot of A4 sample (Zn-20ZnO-9UPP)

4. Conclusion

The electrodeposition of Zn–20ZnO coatings reinforced with unripe plantain peel (UPP) particulates successfully enhanced the structural, mechanical, and corrosion properties of ASTM A795 mild steel. Based on the experimental findings, the following conclusions are drawn:

Corresponding author's email address: ojosundayfayomi3@gmail.com

i. The incorporation of UPP into the Zn–20ZnO coating improved the hardness of the steel substrate from 62.5 HRB for the uncoated specimen to 66.1 HRB for the Zn–20ZnO–9UPP coating, indicating enhanced resistance to surface deformation.
ii. The corrosion performance improved progressively with increasing UPP concentration. The corrosion current density decreased from 1.95×10^{-2} A/cm² for the uncoated steel to 1.52×10^{-2} A/cm² for the Zn–20ZnO–9UPP coating, while the corrosion rate was reduced from 0.0403 mm/yr to 0.0181 mm/yr, representing approximately 55% improvement in corrosion resistance.
iii. The OCP and potentiodynamic polarization results demonstrated that the coated specimens exhibited greater electrochemical stability and lower corrosion activity than the uncoated steel. The reduction in current density observed in the polarization curves confirms that the Zn–20ZnO–UPP coatings effectively suppressed the electrochemical dissolution of the steel substrate.
iv. SEM/EDS analysis confirmed the successful deposition of Zn, ZnO, and UPP-derived constituents on the steel surface, producing a compact and homogeneous coating morphology. XRD analysis further verified the formation of crystalline Zn and ZnO phases together with secondary compounds that contributed to improved coating integrity.
v. Overall, the incorporation of unripe plantain peel particulates into Zn–ZnO coatings produced an environmentally friendly composite coating capable of improving the hardness, structural stability, and corrosion resistance of mild steel, making it a promising surface modification approach for engineering applications.

References

Ajayi, S., Ikubanni, P., Onu, P., Adekanye, TA., Oyewo, AT. and Ajide, O. 2025a. Investigation of corrosion, hardness and wear rate of rice husk-zinc composite coating on A36 steel using dual anode electrolytic deposition technique. Teknomekanik. 8(2):164-182.

Ajayi, SA., Onu, P., Madonsela, NS., Pradhan, A., Ajide, OO. and Oluwole, OO. 2025b. A dual-anode electrolytic codecomposition approach to enhance A36 steel properties with Zn-13, rice husk and white clay coatings. Material Design & Processing Communication. 2025(1): 5415075. https://doi.org/10.1155/mdp2/5415075

Akpan, BJ., Akande, IG., Fayomi, OSI. and Oluwasegun, KM. 2022. Investigation of hardness, microstructure and anti-corrosion properties of Zn-ZnO composite coating doped unripe plantain peel particles. Case Studies in Chemical and Environmental Engineering. 5:100187.

Al-Amiery, AA., Isahak, WNRW. and Al-Azzawi, WK. 2023. Corrosion inhibitors: Natural and synthetic organic inhibitors. Lubricants. 11(4):174.

Antunes, RA., Ichikawa, RU., Martinez, LG. and Costa, I. 2014. Characterization of corrosion products on carbon steel exposed to natural weathering and to accelerated corrosion tests. International Journal of Corrosion. 2014:419570.

Anwar, S., Khan, F., Zhang, Y. and Caines, S. 2021. Zn composite corrosion resistance coatings: What works and what does not work? Journal of Loss Prevention in the Process Industries. 69:104376.

Ates, M. 2016. A review on conducting polymer coatings for corrosion protection. Journal of Adhesion Science and Technology. 30(14):1510-1536.

Ben, F. and Olubambi, PA. 2024. Agro waste reinforcement of metal matrix composites, a veritable sustainable engineering achievement, or an effort in futility? A critical review. Materials Research Express. 11(6):062004.

Draz, U., Waseem, M. and Iqbal, T. 2025. Characterization and corrosion analysis of zinc coating by electrodeposition using acid chloride electrolyte solution. Results in Surfaces and Interfaces. 20:100588.

Fayomi, OS., Adakole, O., Min, HS. and Oluwasegun, KM. 2025. Development and evaluation of modified ZnCr-Shell particulates composite coatings: Corrosion, structural and microhardness properties. Hybrid Advances. 100554.

Corresponding author's email address: ojosundayfayomi3@gmail.com

Fayomi, OSI. 2025. Empirical analysis and mitigation response of synthesised Musa paradisiaca compounds inhibitory extract on AA6063. Solid State Phenomena. 371:81-96.

Fayomi, OSI. and Popoola, API. 2012. An investigation of the properties of Zn coated mild steel. International Journal of Electrochemical Science. 7(7):6555-6570.

Fenker, M., Balzer, M. and Kappl, H. 2014. Corrosion protection with hard coatings on steel: Past approaches and current research efforts. Surface and Coatings Technology. 257:182-205.

Kadhim, A., Al-Amiery, AA., Alazawi, R., Al-Ghezi, MKS. and Abass, RH. 2021. Corrosion inhibitors: A review. International Journal of Corrosion and Scale Inhibition. 10(1):54-67.

Kang, W. and Jin, J. 2026. Corrosion and wear resistance of electro-deposited Zn-Ni/ZnS nanocomposite coatings on mild steel for mechanical applications. Chalcogenide Letters. 23(3).

Luo, X., Yao, Z., Zhang, P. and Gu, D. 2018. Al_2O_3 nanoparticles reinforced Fe-Al laser cladding coatings with enhanced mechanical properties. Journal of Alloys and Compounds. 755:41-54.

Malatji, N., Popoola, API. and Fayomi, OSI. 2017. The effect of nanoparticulate loading on the fabrication and characterization of multi-doped Zn-Al_2O_3-Cr_2O_3 hybrid coatings on mild steel. The International Journal of Advanced Manufacturing Technology. 90:2443-2452.

Marcolin, P., Longhi, M., Zini, LP., Proença, B., de Fraga Malfatti, C., Battisti, LC., Rieder, ES., Zattera, AJ., Kunst, SR. and Oliveira, CT. 2017. Influence of the pH and stirring speed of the electrodeposition bath in the performance of zinc and zinc-nanocomposite coatings. Materials Science Forum. 899:283-288. https://doi.org/10.4028/www.scientific.net/MSF.899.283

Pandit, B., Goda, ES., Shaikh, SF. 2023. Electrochemical deposition toward thin films. In: *Simple Chemical Methods for Thin Film Deposition: Synthesis and Applications*. pp.245-304. Springer.

Phogat, D., Senachamnong, W., Srivastava, A. and Awasthi, S. 2026. Recent advances in Zn-Ceramic nanocomposite coatings for protective interfaces. JOM. 1-26.

Protsenko, VS. 2025. Electrochemical corrosion properties and protective performance of coatings electrodeposited from deep eutectic solvent-based electrolytes: A review. Materials. 18(3):558.

Qi, L. and Kan, H. 2026. Preparation of high-performance Ni-Co-Y_2O_3 coating by optimizing surfactant concentration and its application in nut reinforcement. Results in Surfaces and Interfaces. 22:100687. https://doi.org/10.1016/j.rsurfi.2025.100687

Sajjadnejad, M., Karkon, S. and Haghshenas, SMS. 2024. Corrosion characteristics of Zn-TiO_2 nanocomposite coatings fabricated by electro-codeposition process. Advanced Journal of Chemistry, Section A. 7(2):209-226.

Shibli, SMA., Meena, BN. and Remya, R. 2015. A review on recent approaches in the field of hot dip zinc galvanizing process. Surface and Coatings Technology. 262:210-215.

Thakare, JG., Pandey, C., Mahapatra, MM. and Mulik, RS. 2021. Thermal barrier coatings—A state of the art review. Metals and Materials International. 27(7):1947-1968.

Corresponding author's email address: ojosundayfayomi3@gmail.com